

RESEARCH ARTICLE

Human IL-2R α subunit binding modulation of IL-2 through a decline in electrostatic interactions: A computational and experimental approach

Arezoo Beig Parikhani^{1,2‡}, Kowsar Bagherzadeh^{3,4}, Rada Dehghan^{1,2‡}, Alireza Biglari⁵, Mohammad Ali Shokrgozar⁶, Farhad Riazi Rad⁷, Sirous Zeinali⁸, Yeganeh Talebkhan⁹, Soheila Ajdary^{7*}, Reza Ahangari Cohan^{10*}, Mahdi Behdani^{1*}

1 Venom and Biotherapeutics Molecules Laboratory, Department of Medical Biotechnology, Biotechnology Research Center, Pasteur Institute of Iran, Tehran, Iran, **2** Student Research Committee, Pasteur Institute of Iran, Tehran, Iran, **3** Stem Cell and Regenerative Medicine Research Center, Iran University of Medical Sciences, Tehran, Iran, **4** Eye Research Center, The Five Senses Health Institute, Rassoul Akram Hospital, Iran University of Medical Sciences, Tehran, Iran, **5** School of Medicine, Tehran University of Medical Sciences, Tehran, Iran, **6** National Cell Bank of Iran, Pasteur Institute of Iran, Tehran, Iran, **7** Department of Immunology, Pasteur Institute of Iran, Tehran, Iran, **8** Molecular Medicine Department, Biotechnology Research Center, Pasteur Institute of Iran, Tehran, Iran, **9** Department of Medical Biotechnology, Biotechnology Research Center, Pasteur Institute of Iran, Tehran, Iran, **10** Department of Nanobiotechnology, New Technologies Research Group, Pasteur Institute of Iran, Tehran, Iran

‡ ABP and RD contributed equally to this work as co-first authors

* behdani73042@yahoo.com, behdani@pasteur.ac.ir (MB); cohan_r@yahoo.com (RAC); ajdsoh@pasteur.ac.ir (SA)



OPEN ACCESS

Citation: Beig Parikhani A, Bagherzadeh K, Dehghan R, Biglari A, Shokrgozar MA, Riazi Rad F, et al. (2022) Human IL-2R α subunit binding modulation of IL-2 through a decline in electrostatic interactions: A computational and experimental approach. PLoS ONE 17(2): e0264353. <https://doi.org/10.1371/journal.pone.0264353>

Editor: Michael Massiah, George Washington University, UNITED STATES

Received: August 31, 2021

Accepted: February 8, 2022

Published: February 25, 2022

Peer Review History: PLOS recognizes the benefits of transparency in the peer review process; therefore, we enable the publication of all of the content of peer review and author responses alongside final, published articles. The editorial history of this article is available here: <https://doi.org/10.1371/journal.pone.0264353>

Copyright: © 2022 Beig Parikhani et al. This is an open access article distributed under the terms of the [Creative Commons Attribution License](https://creativecommons.org/licenses/by/4.0/), which permits unrestricted use, distribution, and reproduction in any medium, provided the original author and source are credited.

Abstract

Although high-dose IL-2 has clear antitumor effects, severe side effects like severe toxicity and activation of Tregs by binding of IL-2 to high-affinity IL-2R, hypotension, and vascular leak syndrome limit its applications as a therapeutic antitumor agent. Here in this study, a rational computational approach was employed to develop and design novel triple-mutant IL-2 variants with the aim of improving IL-2-based immunotherapy. The affinity of the mutants towards IL-2R α was further computed with the aid of molecular dynamic simulations and umbrella sampling techniques and the obtained results were compared to those of wild-type IL-2. *In vitro* experiments by flow cytometry showed that the anti-CD25 mAb was able to bind to PBMC cells even after mutant 2 preincubation, however, the binding strength of the mutant to α -subunit was less than of wtIL-2. Additionally, reduction of IL-2R α subunit affinity did not significantly disturb IL-2/IL2R $\beta\gamma$ c subunits interactions.

1. Introduction

Human Interleukin-2 (IL-2) is a pleiotropic cytokine that plays pivotal roles in immune responses [1]. The protein promotes the proliferation, differentiation, and survival of T and B cells, and also enhances the cytolytic activity of natural killer (NK) cells in the innate immune

Data Availability Statement: All relevant data are within the manuscript and its [Supporting Information](#) files.

Funding: This study is supported by a PhD grant from Pasteur Institute of Iran and by grant No: 980902 from the Biotechnology Development Council of the Islamic Republic of Iran to Arezoo Beig Parikhani. The funders had no role in study design, data collection and analysis, decision to publish, or preparation of the manuscript.

Competing interests: The authors have declared that no competing interests exist.

Abbreviations: ConA, Concanavalin A; DSSP, Secondary structure analysis; FDA, Food and Drug Administration; HD-IL-2, High-dose human interleukin-2; IL-2, Human interleukin-2; IL-2R, Interleukin-2 receptor; IFN, Interferon; IPTG, Isopropyl β -D-1-thiogalactoside; M1, Mutant 1 human interleukin-2; M2, Mutant 2 human interleukin-2; Mab, Monoclonal antibodies; MDs, Molecular dynamic Simulations; PBMC, Peripheral blood mononuclear cells; rIL-2, Recombinant wild-type human interleukin 2; RMSD, Root mean square deviations; RMSF, Root mean square fluctuations; SDS-PAGE, Sodium dodecyl sulphate-polyacrylamide gel electrophoresis; TNF, Tumor necrosis factor; Treg, Regulatory T cells; VLS, Vascular leak syndrome; WHAM, Weighted histogram analysis method; wtIL-2, Wild-type human interleukin-2.

defense [2]. IL-2 is a 15-kDa glycoprotein produced primarily by activated CD4⁺ and CD8⁺ T lymphocytes [3]. This cytokine exerts its effect by binding to a heterotrimeric receptor on the surface of immune cells. The high affinity IL-2 receptor is composed of three separate, noncovalently linked subunits, termed IL-2R α (CD25), IL-2R β (CD122), and IL-2R γ c (CD132) [4]. The IL-2R α chain captures IL-2 at the cell surface and delivers it to IL-2R β γ c chains; the signaling part of the receptor [4]. The β and γ c chains are expressed on T cells while the α chain expression is restricted to early thymocytes, Tregs, and activated T cells. While β and γ c chains together form an IL-2 receptor (IL-2R) with intermediate affinity, the α chain is unable to form a functional receptor in the absence of β γ c chains [4].

High-dose (HD) IL-2 was approved by the FDA for the treatment of metastatic renal cell carcinoma in 1992 and metastatic melanoma in 1998 [5]. IL-2 has also been used for the treatment of leukemias and lymphomas [6]. Based on the administered dose of IL-2, it can act as a promoter of both immunosuppression via Tregs, and immune stimulation via other CD4⁺, CD8⁺ T, and NK cells [7]. This dual effect of IL-2 on the immune response limits its applications as a therapeutic antitumor agent [8]. The expression level of IL-2R α on resting cytotoxic lymphocytes, such as NK and CD8⁺ T cells, is low or undetectable, so these cells are not activated by low-doses of IL-2 [9]. IL-2R α expression on these cells increases after the initial stimulation and is required for maximal lymphocyte proliferation. While, high affinity IL-2R on Tregs can compete more effectively for IL-2 at low levels, HD-IL-2 can activate even resting cytotoxic lymphocytes and it is used for immune-stimulatory and antitumor activity [9].

HD-IL-2 administration has been associated with life-threatening toxicities such as vascular leak syndrome (VLS) and pulmonary edema [10], so most patients do not benefit from HD-IL-2 therapy [9]. Lowering IL-2 dose could limit side effects but also decreases the efficacy [11]. It is reported that part of the limitation in IL-2 efficacy for cancer treatment is related to IL-2-driven expansion of Tregs, which leads to a reduced antitumor immunity [12]. An increased level of Tregs has been found in most cancer patients and in cases such as breast cancer, renal cell carcinoma, and non-small cell lung cancer, the increment has been associated with worse disease outcomes or poor survival [13].

Many attempts have been made to improve efficacy of IL-2-based therapy and enhance the safety profile for patients, including; changes in route of administration and combinations with other drugs [3]. However, the issues related to the toxicity and efficacy still remain. Molecular strategies to generate modified forms of IL-2 could be helpful in these areas [7,11]. Therefore, in the current study, we designed and tested a novel triple-mutant IL-2 variant with a reduced affinity to the IL-2R α subunit using a computational approach and experimental analysis.

2. Materials and methods

2.1. Computational studies

The schematic representation of the computational procedure performed in this study is illustrated in [S1 Fig](#).

2.1.1. Design and interaction analysis of IL-2 variants. The X-ray structure of the complex between IL-2 and IL-2 receptor (PDB ID: 2b5i) was retrieved from the protein data bank (<https://www.rcsb.org>). The PDB file was then submitted to PDBsum in the generate mode and the residues involved in hIL2-hIL2R α electrostatic interactions were identified [14]. Then, alanine mutations were applied to the crystal structure of the hIL2-IL-2R α β γ c complex (PDB ID: 2b5i) at the selected positions using Swiss-Pdb Viewer v4.1 [15]. The affinity between IL-2 mutants and IL-2R α -subunit was computed by PRODIGY (<https://nestor.science.uu.nl/prodigy/>) and PDBePISA (<https://www.ebi.ac.uk/pdbe/pisa/>) web servers.

2.1.2. Docking procedure. To predict the best interacting model between IL-2 and the receptor, calculating the approximate binding energy, and obtaining an appropriate initial structure to perform molecular dynamic (MD) simulations, the energy minimized 3D-models were docked over IL-2R $\alpha\beta\gamma$ c using ClusPro webserver [16]. Briefly, all hetero-atoms including waters, ligands, and cofactors were removed. Then, IL-2 and IL-2R $\alpha\beta\gamma$ c were submitted as ligand and receptor, respectively. Finally, the analysis was carried out by defining attraction residues. The docking procedure generated a number of detailed models that were sorted by the cluster size. Finally, the best cluster was chosen according to the predicted binding energies and modes of interactions for further analysis.

2.1.3. Simulations procedure. MD simulations were carried out using GROMACS v5.1.5 software [17] with GROMOS AMBER force field (amber99sb-ildn) [18] on the native and mutated IL-2 [mutant 1 (M1) and mutant 2 (M2)] as well as M1 and M2 structures in complex with IL-2R $\alpha\beta\gamma$ c, for the best-ranked models obtained from the molecular docking studies. The models were solvated in a dodecahedral box of TIP3P water molecules [19] with a minimum distance of 14 Å between the protein surface and the box wall. The net charge of the system was neutralized by replacing water molecules with appropriate counter sodium and chloride ions. The van der Waals cutoff was set to 14 Å. Periodic boundary conditions were assigned in all directions. The solvated system was then minimized through the steepest descent algorithm [20] with 1000 KJ mol⁻¹ nm⁻¹ tolerance followed by a canonical ensemble (NVT) and isothermal-isobaric ensemble (NPT) for 20 ps. The temperature and pressure of the system were independently maintained using Berendsen thermostat and Parrinello-Rahman barostat algorithm [21] at constant temperature and pressure of 300 K and 1 bar, respectively. The particle mesh Ewald (PME) algorithm was employed to calculate the long-range electrostatic interactions [22]. The LINCS algorithm [23] was applied to restrain all the bonds with an integration step of 1 fs. Finally, the whole system was subjected to 100 ns of MDs at constant pressure and temperature. The stability of the computed structures was investigated by calculating the root mean square deviations (RMSD) and root mean square fluctuations (RMSF) during the simulation. The coordinate files were finally extracted from the trajectories for further analysis.

2.1.4. Umbrella sampling procedure. An umbrella sampling algorithm was employed to calculate potentials of mean force (PMF) [24]. The average structure from the last 40 ns of each simulation was selected for the umbrella sampling study to calculate the potential of mean force (PMF) for the native and mutant complexes. The already equilibrated complexes were first made parallel to the z-axis. A constant velocity pulling procedure with a rate of 1 nm was assigned to pull IL-2R α along the z-axis by a 6.0 nm distance. Therefore, a box was constructed with a z-axis length of 12 nm. The prepared box was solvated, neutralized, minimized, and equilibrated at a temperature (NVT) and specific pressure (NPT) similar to the previous MD simulations. The umbrella sampling simulation began with the center-of-mass-pulling method. IL-2R α was pulled from the complex towards the solvent bulk over the course of 500 ps by using a 1000 kJ/(mol*nm) force, at the rate of 0.01 nm per ps. During this simulation, snapshots were saved at each 10 ps, so in total 50 configurations were generated from the pulling simulations. Eventually 22 to 23 configurations with a spacing of 0.2 nm were obtained for each complex to ensuring sufficient overlap of the probability distribution of each configuration. The selected configurations were then used as the starting configurations for each umbrella sampling simulation and were subjected to 1 ns of MDs after a brief NPT equilibration, independently. The potential mean force (PMF) was calculated using the weighted histogram analysis method (WHAM) [25]. The binding free energy (ΔG) was calculated for each system by taking the difference between the plateau region of the PMF curve and the energy minimum of each simulation.

2.1.5. Data analysis and graphical presentation. The MDs results were analyzed and visualized with Schrödinger and Pymol packages [26,27]. The graphs were all represented visually by using Microsoft Office Excel.

2.2. Experimental studies

2.2.1. Protein expression, identification, and purification. For the expression of native and mutant IL-2 (M2), the synthetic genes encoding the wild and M2 IL-2 were subcloned separately into pET28a expression vector using *Nco*I and *Hind*III restriction sites. The expression vectors were transformed into *E. coli* BL21 (DE3) strain using the heat shock method. Transformed clones were inoculated into 200 ml Luria Broth (LB) medium supplemented with 50 μ g/mL kanamycin. The protein expressions were induced with 0.5 mM isopropyl β -D-1-thiogalactoside (IPTG) (Sigma, USA) at an OD 600nm of 0.5 and the bacterial pellet was collected 6 hours post-induction by centrifugation at 6000 rpm for 20 minutes and subjected to 12% SDS-PAGE to analyze the protein expression.

For western blotting, the proteins were transferred onto nitrocellulose membrane using Semi-Dry Transfer system (Bio-Rad, USA) for 45 min at 200 mA. The membrane was blocked in 3% skimmed milk in PBS for 2 h at room temperature and then incubated overnight with 1:2000 dilution of rabbit anti-Histidine primary antibody at room temperature. After 3 times washing with PBS-tween20 0.05%, the membrane was incubated with 1:2000 goat anti-rabbit HRP-conjugated secondary antibody (Sigma, USA) for 4 h. Finally, the membrane was washed 3 times similar to the previous step and stained using 3,3'-diaminobenzidine (DAB) substrate.

For protein purification, the bacterial pellets were resuspended in lysis buffer (10 mM imidazole, 0.5 M NaCl, 50 mM NaH₂PO₄; pH8.0) and sonicated at an amplitude of 100% (30-sec pulses with 10-sec intervals, for 10 min). The lysates were then centrifuged at 10,000 g for 20 min. The pellet, containing inclusion bodies (IBs), was solubilized in solubilization buffer (8M urea, 50 mM NaH₂PO₄, 300 mM NaCl, 10 mM imidazole) and placed under agitation for 1h at room temperature. After centrifugation (10,000 g for 30 min), the supernatant was filtered by 0.45 μ m filters and applied to Ni-NTA resin at a low flow rate (1 ml/min). The recombinant protein was refolded on the column through a gradual removal of urea (from 8M to 0) by the refolding buffer (50 mM NaH₂PO₄, 0.5 M NaCl, 20 mM Imidazole; pH 8.0) over a period of 2 h. The His6-tagged proteins were eluted with the elution buffer (250 mM imidazole, 50 mM NaH₂PO₄, 0.5 M NaCl; pH 8.0). The purity of refolded soluble elution fractions was analyzed using 12% SDS-PAGE.

2.2.2. PBMC isolation, stimulation, and flow cytometry. Human peripheral blood mononuclear cells (PBMC) were separated from a healthy blood donor using Ficoll-Hypaque (Lymphodex, Innotrain, Germany) by density gradient centrifugation at 400 g at room temperature for 30 min according to the manufacturer's protocol. The cells were washed three times with sterile phosphate-buffered saline (PBS), counted, and resuspended in RPMI medium supplemented with 10% fetal bovine serum (FBS), 2 mM L-glutamine, 100 U penicillin, and 100 μ g streptomycin defined as complete medium (CM). For the induction of CD25 expression, PBMCs were stimulated with 5 μ g/ml concanavalin A (ConA) for 24 h. After washing with PBS, the cells were incubated with IL-2 or IL-2 mutein in CM for 24 h. His-tagged recombinant proteins bound-cells were detected with rabbit anti-His-tag Ab and mouse anti-rabbit FITC-conjugated. In another experiment, the cells previously incubated with wtIL-2 and M2, were stained with anti-CD25 MAb-PE antibody (eBioscience, United States). After adequate washing, flow cytometry was performed using Partec PAS III flow cytometer (Partec GmbH, Gorlitz, Germany), and data were analyzed by FlowJo software (Tree Star, Inc., Ashland, OR, USA). Isotype-matched control antibodies were used to detect non-specific binding to the cells.

3. Results

3.1. Computational studies

3.1.1. Residue identifications. The overall structure of IL-2 is presented in Fig 1A. Analyzing the interactions between IL-2 and IL-2R α revealed that residues K35, R38, F42, K43, Y45, E61, E62, P65, L72, and Y107 are involved in the electrostatic interactions with IL-2R α . While residues E61, E62, P65 and L72 and Y107 are located in a loop structure (A-B loop and C-D loop, respectively), the other target residues are constituents of β sheets and α helices. To generate the initial structure of IL-2/IL-2R complex, the target residues were individually mutated to alanine using Swiss-Pdb Viewer v4.1 (15). The affinity between IL-2 mutants and IL-2R α subunit was evaluated with the aid of PRODIGY (<https://nestor.science.uu.nl/prodigy/>) and PDBePISA (<https://www.ebi.ac.uk/pdbe/pisa/>) web servers. By keeping default parameters, the dissociation constants (K_d) and binding affinity (ΔG) were finally calculated at 25°C. Based on the obtained *in silico* affinity measurements, three mutations that had more impact on the affinity reduction of IL-2R α subunit were selected (S1 Table). The results obtained from PRODIGY showed that 8 out of 9 single amino-acid substitutions increased binding energy relative to wtIL-2, among which K35A, F42A, and E61A resulted in higher binding free energies and eventually larger reduction in binding affinity for IL-2R α in comparison to other mutations and wtIL-2. Also, PISA analysis revealed that F42A, P65A, and L72A would lower the binding affinity for IL-2R α in comparison to the rest of the assigned mutations as well as wtIL-2. Therefore, two variants of triple mutant F42A, P65A, and L72A as mutant 1 (M1) and K35A, F42A, and E61A as mutant 2 (M2) were designed.

3.1.2. In Silico characterization of the designed variants. The designed variants as well as the wtIL-2 were submitted to a comprehensive set of atomistic MD simulations to investigate how the assigned mutations would alter the native structure of the target protein, IL-2, and predict appropriate conformations of the variants for predicting their interactions with IL-2R $\alpha\beta\gamma$. The obtained results were analyzed as the time evolution in detail for the native and mutant conformations. Basic MD simulation trajectory analysis, including root mean square deviation (RMSD), root mean square fluctuation (RMSF), and the secondary structure analysis (DSSP) were performed for wtIL-2 as well as M1 and M2 as the time evolution of the native and mutant conformations using GROMACS software.

The backbone RMSD plots of the target structures showed that wtIL-2 and M2 trajectories become stable after almost 38 ns and 55 ns of simulations, respectively, while for that of M1, it becomes stable after 45 ns of simulations and stays flat up to nanosecond 80 ns and then decrease and stay stable for the 10 ending nanoseconds of simulation time (Fig 1B). Totally, the root mean structure deviations of the target structures are less than 0.2 nm which shows probably no significant structural rearrangements like refolding of a helix into a loop or a β -sheet to a turn has occurred.

The per-residue root mean-square fluctuation (RMSF) plots of the wild and mutated types of IL-2 are presented in Fig 1C. The obtained results revealed that substitution of K35A decreased fluctuation in α helix for M2, while F42A and E61A behave like those in wtIL-2 structure (Fig 1D and 1E). In contrast, F42A, and L72A showed an increase in A-B loop and B helix fluctuations in comparison to wtIL-2 and M2 that can be attributed to the loss of π - π stack electrostatic interactions between P65, F42 and F43 (Fig 1F) and polar interactions between L72 and R38 (Fig 1G) due to alanine substitution. Also, the RMSF plots elucidated that M1 and M2 show fluctuation behaviors close to that of wtIL-2 which reveals the structural stability of the two mutants relative to the wtIL-2.

The structure of the wild type and mutants were further assessed employing secondary structure analysis (Fig 2). The obtained results show no significant refolding in the percent of

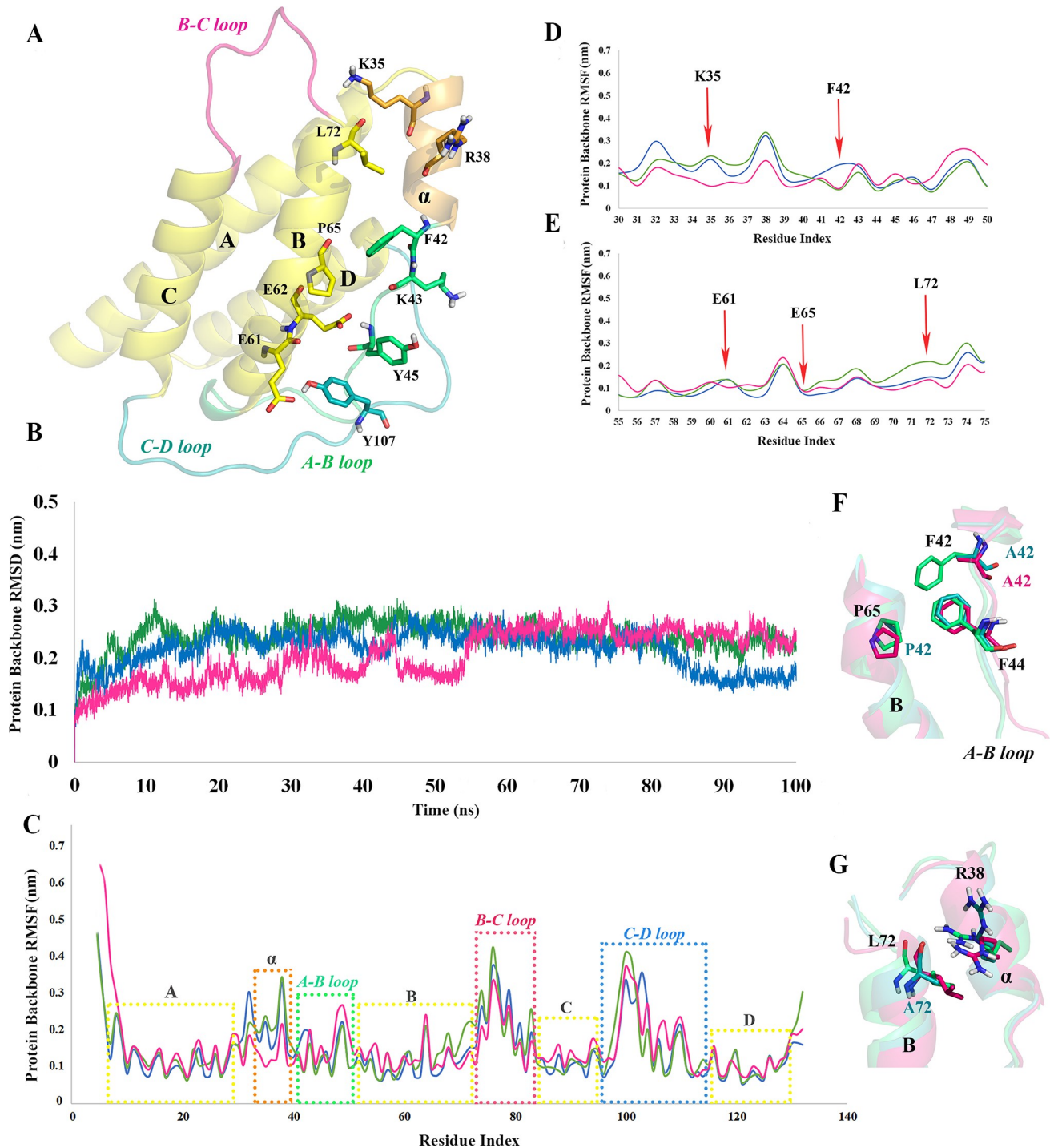


Fig 1. A. IL-2 protein structure (hot spot residues in sticks), B. Back-bone root mean square fluctuations (RMSD) of the native (green), mutant 1 (blue) and mutant 2 (magenta) protein, C. Per-residue root mean square fluctuations (RMSF) of the native (green), mutant 1 (blue) and mutant 2 (magenta) protein residues, D. Per-residue root mean square fluctuations (RMSF) of the target residues 30–50 close view, E. Per-residue root mean square fluctuations (RMSF) of the target residues 55–75 close view, F. Residues F42, F43 and P65, and g. Residues L72 and R38.

<https://doi.org/10.1371/journal.pone.0264353.g001>

residues participating different structural arrangements (Fig 2A–2C). According to Fig 2D–2F, the assigned mutations has decreased the number of α -helix participating residues from 55%

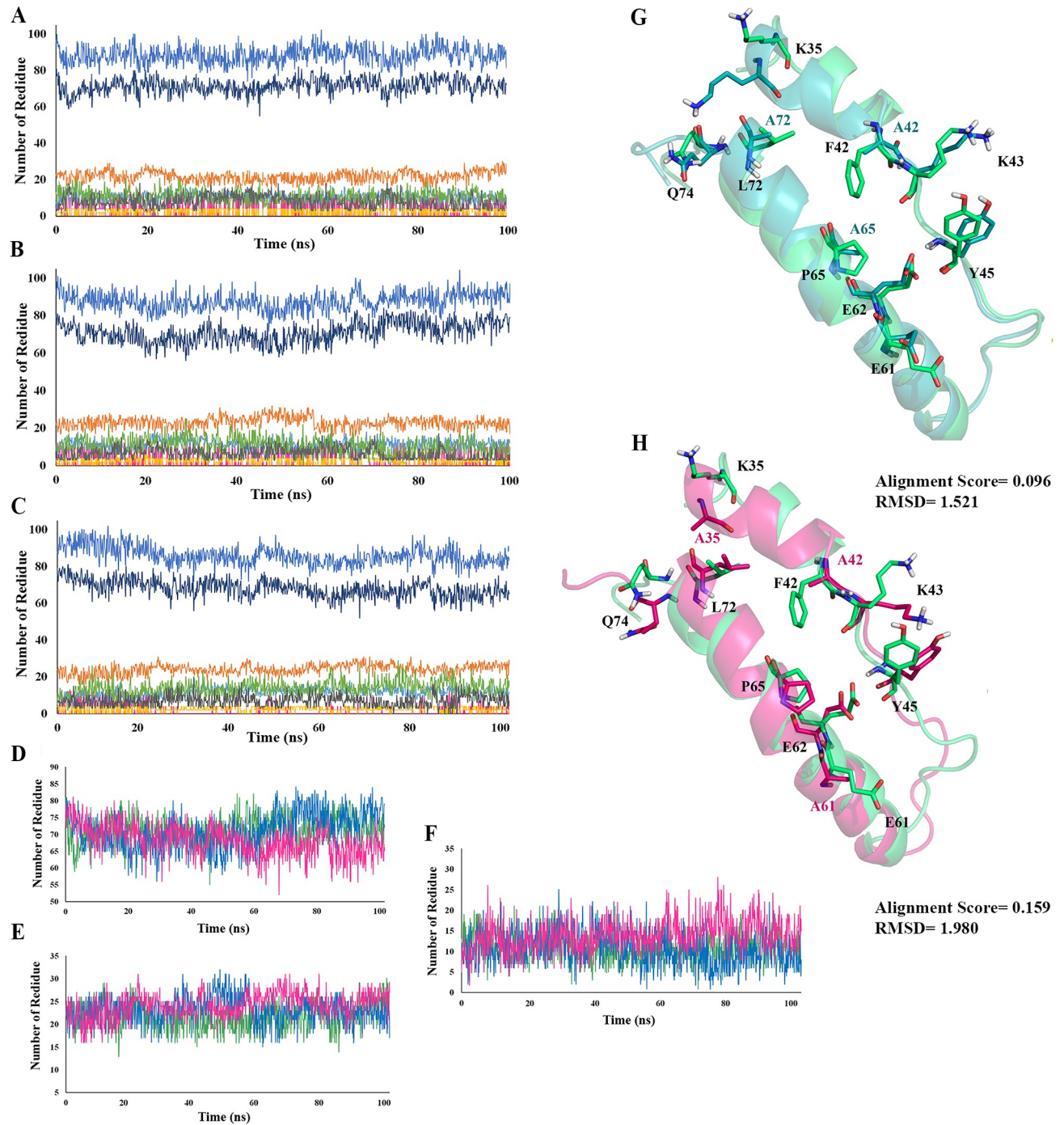


Fig 2. Secondary structure analysis. **A.** The native protein, **B.** Mutant 1 and, **C.** Mutant 2, during 100 ns of MDs (where the structure is shown in blue, α -helix in dark blue, 3-helix in gray, coil in orange, turn in green, β -sheet in magenta, b-bridge in yellow, and bend in cyan), **D.** α -helix structure of native structure (green), mutant 1 (blue) and mutant 2 (magenta), **E.** Coil structure of native structure (green), mutant 1 (blue) and mutant 2 (magenta), **F.** Turn structure of native structure (green), mutant 1 (blue) and mutant 2 (magenta), **G.** superimposition of the native IL-2 and IL-2R α interacting residues over mutant 1, and **H.** superimposition of mutant 2 and IL-2R α interacting residues over mutant 2 IL-2.

<https://doi.org/10.1371/journal.pone.0264353.g002>

in wtIL-2 and M1 to 53% in M2, and increased the number of the coil and turn participating residues from 8% and 18% in wtIL-2 and M1 to 11% and 19% in M2, respectively. Additionally,

the average structures of the computed mutants were obtained from the plateau of the MD simulation and aligned over that of wtIL-2 (Fig 2G and 2H) and alignment scores of 0.096 and 0.159 and also RMSD values of 1.521 and 1.980 Å were obtained for M1 and M2 over wtIL-2, respectively.

Ramachandran Plot server (<https://zlab.umassmed.edu/bu/rama/>) was used to evaluate the reliability of the modeled mutants and as an energetic visualization of allowed and disallowed dihedral angles psi (ψ) and phi (ϕ) of amino acids (S2 Fig). The obtained results showed that the percent of the residues in the favored region are 95.33%, 95.16%, and 94.81% as well as 3.80%, 3.80%, and 4.15% in the allowed region for wtIL-2, M1 and M2, respectively, after 100 ns of simulation (S2 Table). Also, the number of residues in the disallowed region are obtained to be 0.865%, 1.036%, and 1.038% for wtIL-2, M1, and M2, respectively. Ramachandran plots demonstrated that the 3D modeled structures of the mutants represent favorable features, indicating the total percentage of favored and allowed region residues are more than 98%. Since the presence of more than 90% of the residues in the favored and allowed regions of the plot are considered ideal, the quality of the overall structures was desirable enough to be used for the upcoming computational studies [28].

3.1.3. Docking studies. Docking studies were conducted to predict the best interacting model between IL-2 and IL-2R $\alpha\beta\gamma$, calculate an approximate binding energy, as well as obtaining an appropriate mode of interactions for MD simulations. Therefore, the average structures of the computed wt-IL2 and mutants obtained from 100 ns of simulations were used as the structure to be docked over IL-2R $\alpha\beta\gamma$ with the aid of ClusPro webserver (16). The interacting residues were assigned to the webserver and the best-ranked models of complexes were selected considering the type of interactions (mainly hydrogen bonds, hydrophobic and electrostatic interactions), the interacting residues, orientations, distance and the binding energies. The binding affinity (the dissociation constant, K_d) of the obtained complexes were predicted using PRODIGY webserver (Table 1). It is observed that R38A, F42A, and E61A substitutions considerably decrease the affinity of M2 for IL-2R α in comparison to wtIL-2 and M1. To ensure that the decrease in the affinity is a result of a decline in the target residues interactions with IL-2R α , wtIL-2 and the variants affinity for IL-2R β and IL-2R γ were also studied by PRODIGY (S3 Table). The obtained results showed that the affinity of M2 for IL-2R α decreases while increases the affinity of the mutant for IL-2R β . The assigned mutations affect the affinity of the M2 for IL-2 γ . Since the IL-2R γ binding site is close to that of IL-2R α , mutations in the latter would probably induce conformational changes in the former site.

3.1.4. Molecular dynamic simulations of the complex structures. The top rank complexes obtained from docking studies were subjected to molecular dynamic simulations for 100 ns to check the stability of the docked structures as well as the observed interactions. The backbone root mean square deviations were computed individually for IL-2 and the variates as well as IL-2R α , IL-2R β , and IL-2R γ and are presented in Fig 3. RMSD plots of IL-2R β (Fig 3A) and IL-2R γ (Fig 3B) reach the plateau after 15 ns and 5 ns, respectively, with RMSD values less than 0.1 nm, which shows the stability of their structures as well as their interactions with IL-2 and mutants M1 and M2. These phenomena further confirm that the alternations observed in the docking binding energies are due to the made mutations. Considering the RMSD plot of IL-2R α (Fig 3C), the plot became stable after 30 ns of MDs and stayed steady

Table 1. The binding and docking energy comparison between wtIL-2, M1, and M2 complexes.

	wtIL-2	M1	M2
Cluspro Docking (kcal/mol)	-3935.1	-3510.7	-3410.9
The Prodigy analysis (the dissociation constant (K_d) M)	2.6×10^{-8}	2.6×10^{-8}	1.2×10^{-7}

<https://doi.org/10.1371/journal.pone.0264353.t001>

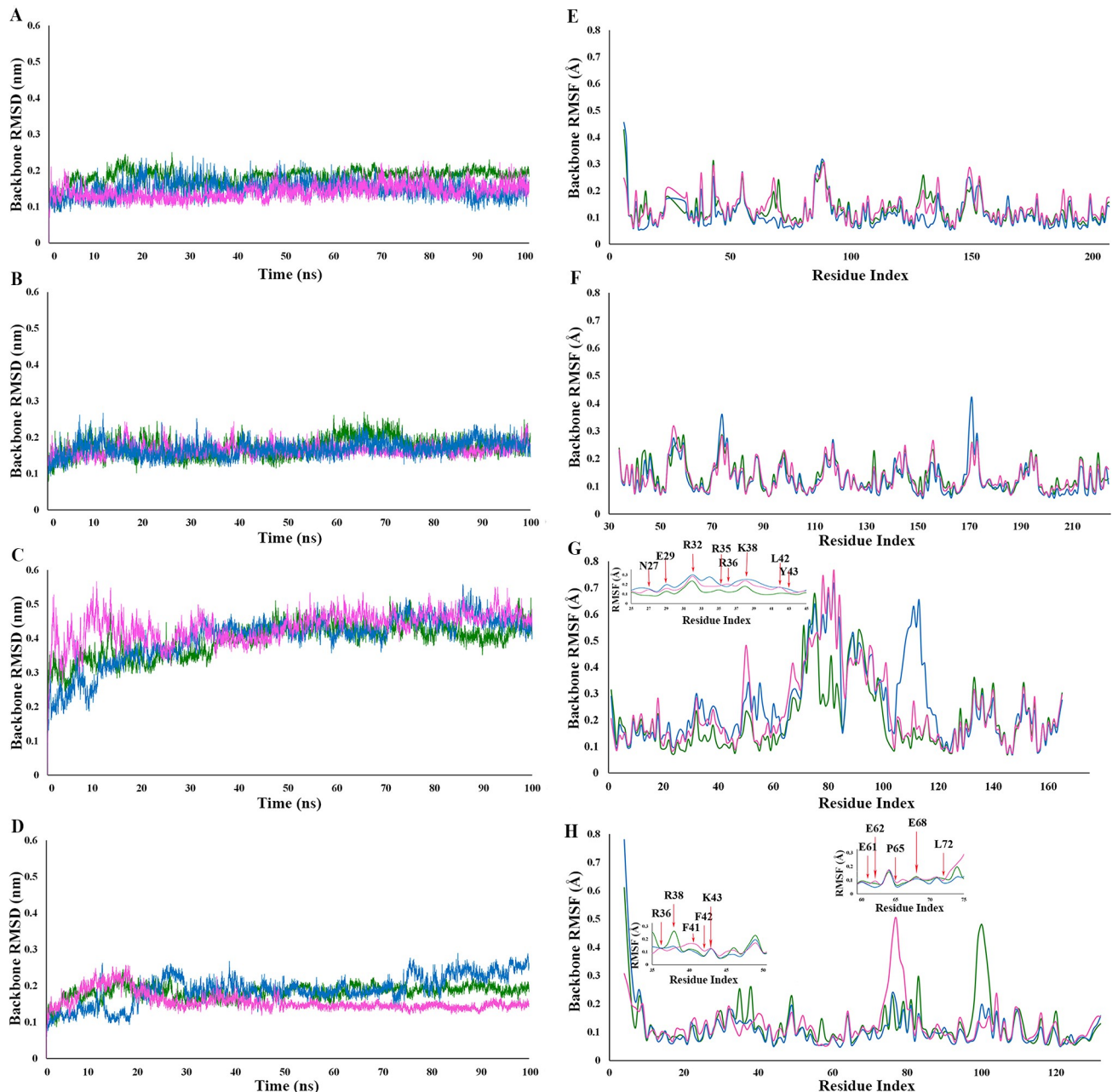


Fig 3. Back-bone root mean square fluctuations (RMSD). A. IL-2R β (the native (green), mutant 1 (blue) and mutant 2 (magenta) proteins), B. IL-2R γ (the native (green), mutant 1 (blue) and mutant 2 (magenta) proteins), C. IL-2R α (the native (green), mutant 1 (blue) and mutant 2 (magenta) proteins), and D. Native IL-2 (green), mutant 1 (blue) and mutant 2 (magenta) proteins during 100ns of MDs. Back-bone root mean square fluctuations (RMSF) of, E. IL-2R β residues (the native (green), mutant 1 (blue) and mutant 2 (magenta) proteins), F. γ c residues (the native (green), mutant 1 (blue) and mutant 2 (magenta) proteins), G. IL-2R α residues (the native (green), mutant 1 (blue) and mutant 2 (magenta) proteins), and H. wtIL-2 residues (green), mutant 1 (blue) and mutant 2 (magenta) during 100ns of MDs.

<https://doi.org/10.1371/journal.pone.0264353.g003>

during the rest of the simulation. While the RMSD value was less than 0.1 nm and 0.15 nm for IL-2R α in complex with wtIL-2 and M1, respectively, sharp jumps with RMSD values more than 0.3 nm were observed for the subunit in complex with M2. It shows that IL-2R α face significant structural rearrangements to be able to establish new interactions or loose interactions with M2, which is also evident in the RMSD plot of M2 in complex with IL-2R α β γ c (Fig 3D).

Table 2. Main interactions observed between wtIL-2, M1, and M2 mutants with IL-2R α During 100ns of MDs.

IL-2 Residues	IL-2R α Residues	Distance	Specific Interactions	HB	Salt bridge	Surface Complementarity	Buried SASA
K35	E1 D4	2.7 Å 4.0 Å	1x hb, 1x salt bridge to E1	1	1	0.76	71.1%
R38	F121 C3 H120 D4	3.0 Å 3.1 Å 3.5 Å 3.9 Å	1x hb to F121	1	0	0.86	80.6%
T41	N27 I118 H120	3.3 Å 3.9 Å 3.9 Å	1x hb to N27	1	0	0.85	61.6%
F42	H120 N27 L42	3.1 Å 3.6 Å 3.7 Å	1x π -alkyl to L42	0	0	0.76	99.8%
K43	R36 E29	2.7 Å 3.5 Å	1x hb, 1x salt bridge to E29 1x hb to R36	2	1	0.44	53.0%
F44	R36	3.5 Å	1x π -alkyl R36	0	0	0.65	93.1%
Y45	R35 R36	3.5 Å 3.5 Å	1x π -alkyl, 1x π -cation to R35 1x π -alkyl to R36				
E61	R35 K38	2.7 Å 3.6 Å	1x hb, 1x salt bridge to R35	1	1	0.51	80.3%
E62	R36	2.7 Å	2x hb, 1x salt bridge to R36	2	1	0.50	97.0%
P65	R36	3.3 Å	1x π -alkyl to L42	0	0	0.79	98.7%
E68	Y43 L42	2.6 Å 3.7 Å	1x hb to Y43	1	0	0.86	60.1%
L72	M25 Y43	3.7 Å 3.5 Å	1x π -alkyl to Y43	0	0	0.44	63.8%
Y107	S64 R35	2.9 Å 3.2 Å	1x hb to S64	1	0	0.79	96.4%
E110	R32	2.7 Å	2x hb, 1x salt bridge to R32	2	1	0.86	39.0%
M1 Residues	IL-2R α Residues	Distance	Specific Interactions	HB	Salt bridge	Surface Complementarity	Buried SASA
A42	L42	4.0 Å	—	0	0	0.41	100%
E61	S39 K38	2.7 Å 2.8 Å	1x hb, 1x salt bridge to K38 1x hb to S39	2	1	0.71	71.9%
E62	R36 S39 R35 K38	2.7 Å 2.8 Å 2.8 Å 3.9 Å	1x hb to R35 2x hb, 1x salt bridge to R36 1x hb to S39	4	1	0.65	94.6%
A65	G40 R36	3.6 Å 3.7 Å	—	0	0	0.81	98.0%
E68	Y43	2.8 Å	1x hb to Y43	1	0	0.29	38.6%
A72	Y43	3.5 Å	—	0	0	0.87	60.8%
M2 Residues	IL-2R α Residues	Distance	Specific Interactions	HB	Salt bridge	Surface Complementarity	Buried SASA
A42	N27	3.7 Å	—	0	0	0.77	100.0%
A61	S39 K38	3.0 Å 3.9 Å	1x hb to S39	1	0	0.52	82.0%
E62	R35	3.8 Å	1x hb to R35	0	1	0.15	91.6%
E68	Y43 S41	2.5 Å 2.7 Å	1x hb to S41 1x hb to S43	2	0	0.66	61.7%

<https://doi.org/10.1371/journal.pone.0264353.t002>

Accordingly, the RMSD plots of IL-2 and M2 reach the plateau after 20 ns of simulations with RMSD values less than 0.1nm, but for that of M1, the plot reaches the steady-state after 30 ns of simulations with RMSD value of 0.1 nm, but starts to increase from nanosecond 80 and

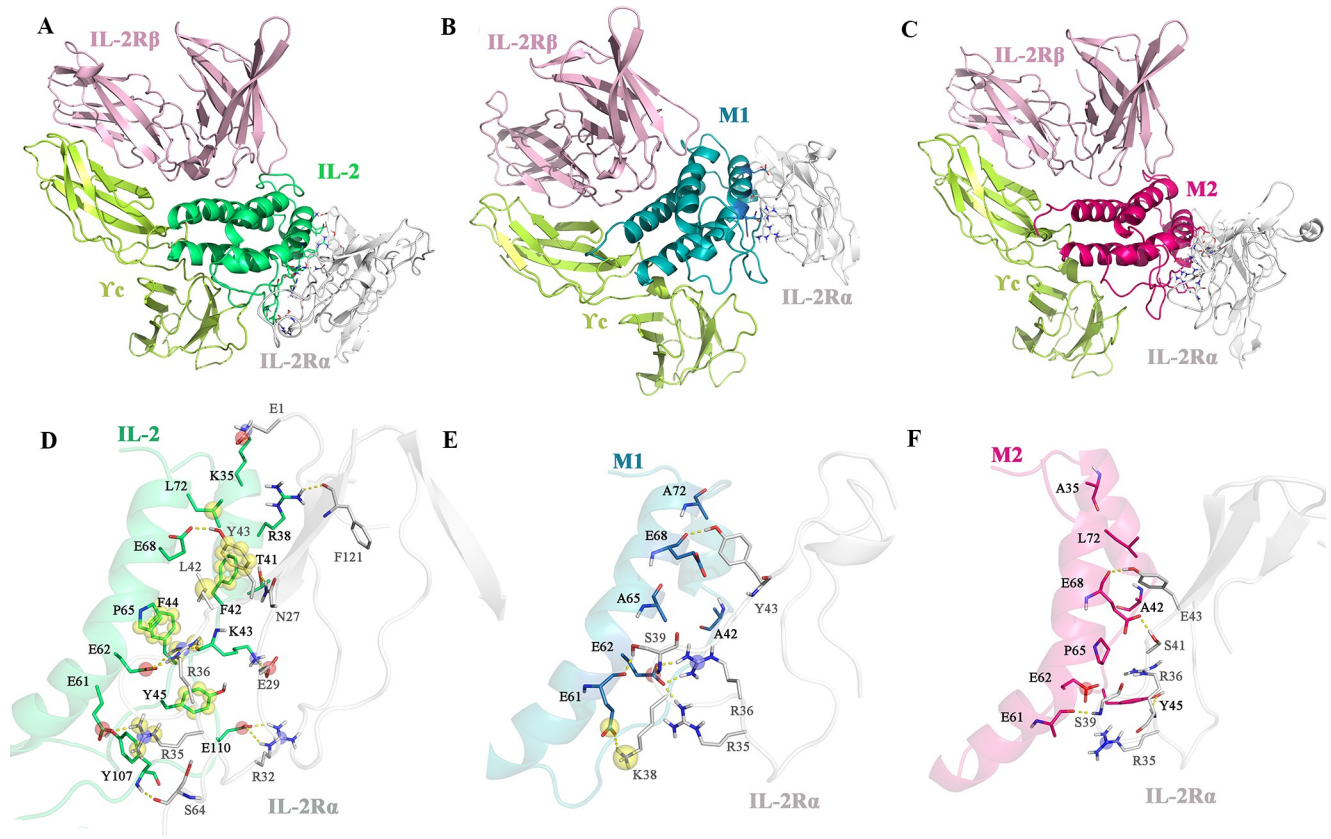


Fig 4. Interactions between **A.** wtIL-2 and IL-2R α β γ c, **B.** M1 and IL-2R α β γ c, and **C.** M2. IL-2R α β γ c after 100 ns of MDs, as well as the close view of **D.** wtIL-2 and IL-2R α interactions, **E.** M1 and IL-2R α and **F.** M2 and IL-2R α . The hydrogen bonds are shown in yellow dashes. The red and blue spheres represent charging interactions (salt bridges), and the yellow spheres represent electrostatic (like π - π , alkyl- π and π -cation) interactions.

<https://doi.org/10.1371/journal.pone.0264353.g004>

reach the plateau again in nanosecond 90 and stay steady for the rest of the simulation time. This shift in M1 RMSD plot can be referred to as the decrease in its affinity for IL-2R β and IL-2R γ c besides IL-2R α , while the decline in M2 affinity for IL-2R α enhances its interactions with the two other subunits (Fig 3).

The per-residue root mean-square fluctuation (RMSF) plots of IL-2R β and IL-2R γ c further confirms the stability of their interactions and conformation in complex with IL-2 and the mutants (Fig 3E and 3F). The RMSF plots of IL-2R α in complex with M1 and M2 showed a non-significant increase (less than 0.1 nm) in the interacting residues fluctuations which is due to the loss of interactions with the mutants in comparison with IL-2 (Fig 3G). Also, the RMSF plots of IL-2, M1, and M2 show that the assigned mutations do not alter the native protein structure drastically. Since residues E61 to L72 are located in the B helix structure and substitution with alanine does not alter main chain interactions, notable fluctuations are avoided in the region. Also, fluctuations in F41A and F42A are because of their being involved in coil structure which is less than 0.1 nm (Fig 3H).

Interactions between IL-2, M1, and M2, with IL-2R α were thoroughly studied with the application of Schrodinger software. According to Table 2 and Fig 4A, wtIL-2 interacts with IL-2R α through hydrogen bond and salt bridge formation between residues K35, R38, T41, K43, E61, E62, E68, Y107, and E110 with residues E1, N27, E29, R32, R35, R36, Y43, S64, and F121, but no pi-stacking interactions are observed between the two proteins. The interactions are drastically reduced between M1 and M2 residues with IL-2R α . While M1 forms hydrogen

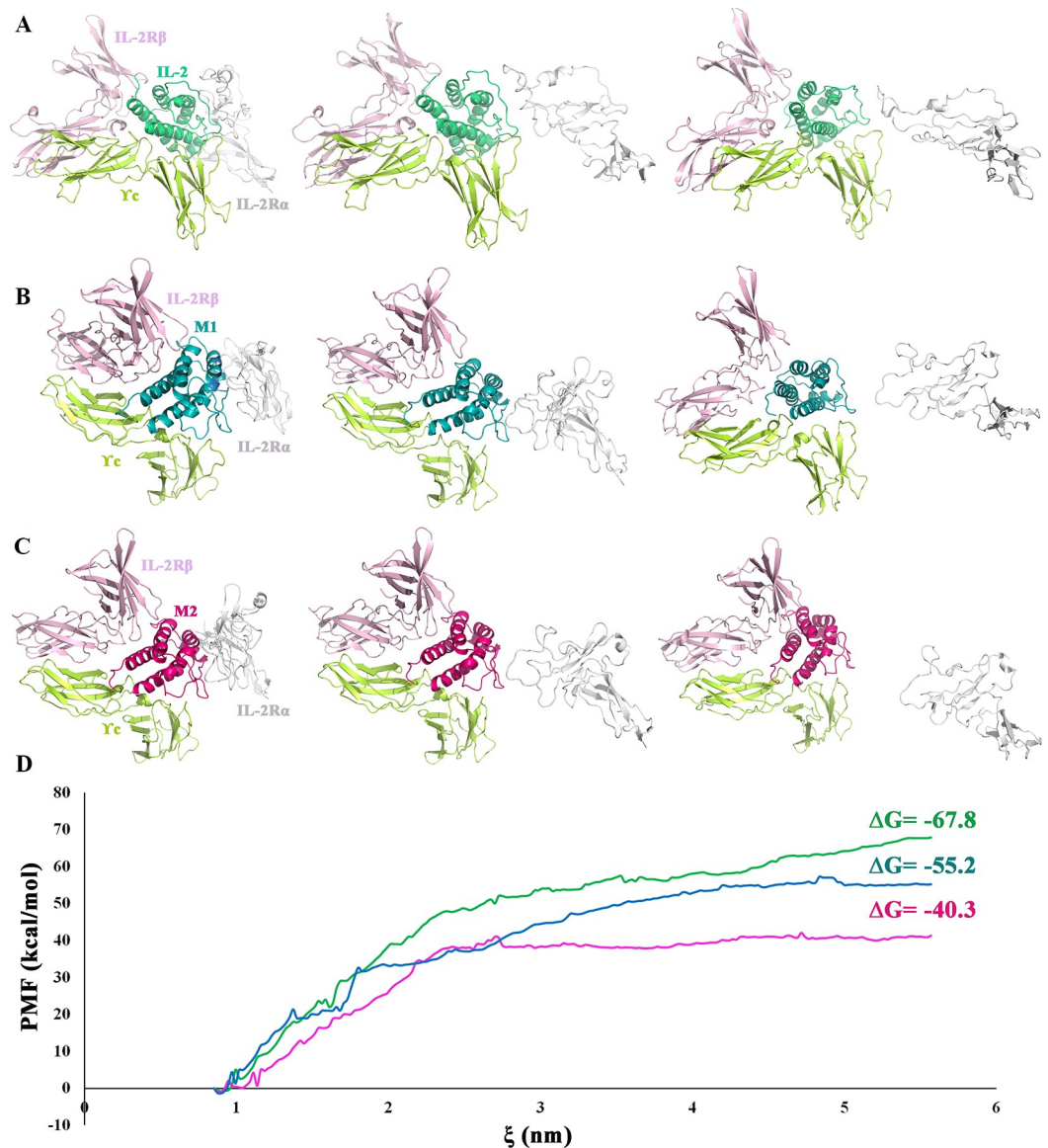


Fig 5. Snapshots of umbrella sampling simulations of the target complex. A. Native IL-2, B. Mutant 1 and C. Mutant 2. D. Potentials of mean forces (PMF) for IL-2 and IL-2R α (the native (green), mutant 1 (blue) and mutant 2 (magenta) proteins) as a function of the reaction coordinate (ξ).

<https://doi.org/10.1371/journal.pone.0264353.g005>

bonds and salt bridges with R35, R36, K38, S39, and Y43, M2 only forms hydrogen bonds with residues R35, S39, S41, and S43 (Fig 4B and 4C).

Furthermore, the alternation in the number of hydrogen bonds between wt-IL2, M1, and M2 with IL-2R β , IL-2R γ_c , and IL-2R α were calculated during 100 ns of MDs (S3 Fig). Accordingly, while the number of hydrogen bonds between M2 and IL-2R α is the least in comparison with those of wtIL-2 and M1, the interactions are almost constant for those of IL-2R β and IL-2R γ_c in complex with M2. Although the focus of this study was to decrease the electrostatic interactions between IL2 and IL-2R α , the stability in the number of hydrogen bonds between the mutants and IL-2R β and IL-2R γ_c shows that the mutations did not disturb the target protein interactions with the IL2R. $\beta\gamma_c$.

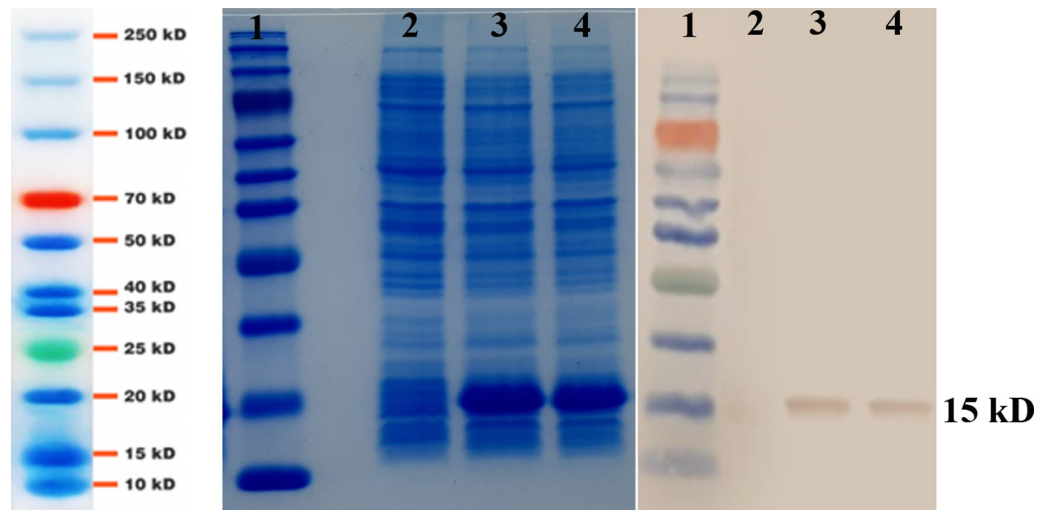


Fig 6. SDS-PAGE and Western blotting analysis of the recombinant proteins. Lane 1, protein marker (10–250 kDa). Whole lysate of BL21(DE3)-pET-22b without gene (lane 2), expressed wtIL-2 (lane3), mutant IL-2 (lane4).

<https://doi.org/10.1371/journal.pone.0264353.g006>

3.1.5. Umbrella sampling. To calculate the binding free energy (ΔG) of the wtIL-2-ILR2 $\alpha\beta\gamma$, M1-hILR2 $\alpha\beta\gamma$, and M2-hILR2 $\alpha\beta\gamma$, IL-2R α was assigned a constant velocity pulling procedure followed by umbrella sampling simulations. PMF curves were obtained from simulations of 23 windows for each system as a function of the distance between centers of mass (COMs) of wtIL-2, M1, and M2 and IL-2R α using the weighted histogram analysis method (WHAM) (S4 Fig). According to Fig 5, wtIL-2 more strongly binds to IL-2R α with a ΔG value of -67.8 kcal/mol in comparison with M1 and M2, indicating a stronger binding between wtIL-2 and IL-2R α . Additionally, M2 with a ΔG value of -40.3 kcal/mol has the least affinity for IL-2R α . Eventually, mutant 2 was selected for further experimental evaluations.

3.2. Experimental studies

3.2.1. Protein expression and purification. 12% SDS-PAGE and western blotting analyses confirmed the presence of approximately 15 kDa band for wild and M2 IL-2 in the crude and purified samples (Fig 6).

3.2.2. Flow cytometry. We used flow cytometry to evaluate the capacity of the new molecule to bind to the ConA activated PBMCs, which express high levels of trimeric IL-2R [29]. At equal concentration, the mean fluorescence intensity (MFI) was obtained 8.99 and 13.80 for the M2 and wtIL-2, respectively, showing the binding capacity of M2 was lower than wtIL-2 (Fig 7A). A competitive binding assay was also performed to determine whether the M2 can inhibit the binding of the anti-CD25 mAb, which competes with wtIL-2 (Fig 7B). The results indicated that the MFI value for the PBMCs which were preincubated with M2 was almost the same as the un-incubated cells (21.1 vs. 21.8, respectively); while, the pre-incubation of cells with wtIL-2 decreased the MFI to 10.2.

4. Discussions

Considered the first effective cancer immunotherapy, HD-IL-2 therapy has a response rate of approximately 20% in patients with metastatic melanoma and renal cell cancers. However, high dose IL-2 treatment resulted in an unwanted expansion of immunosuppressive Tregs through preferential binding of IL-2 to the high-affinity IL-2R, which have limited the efficacy

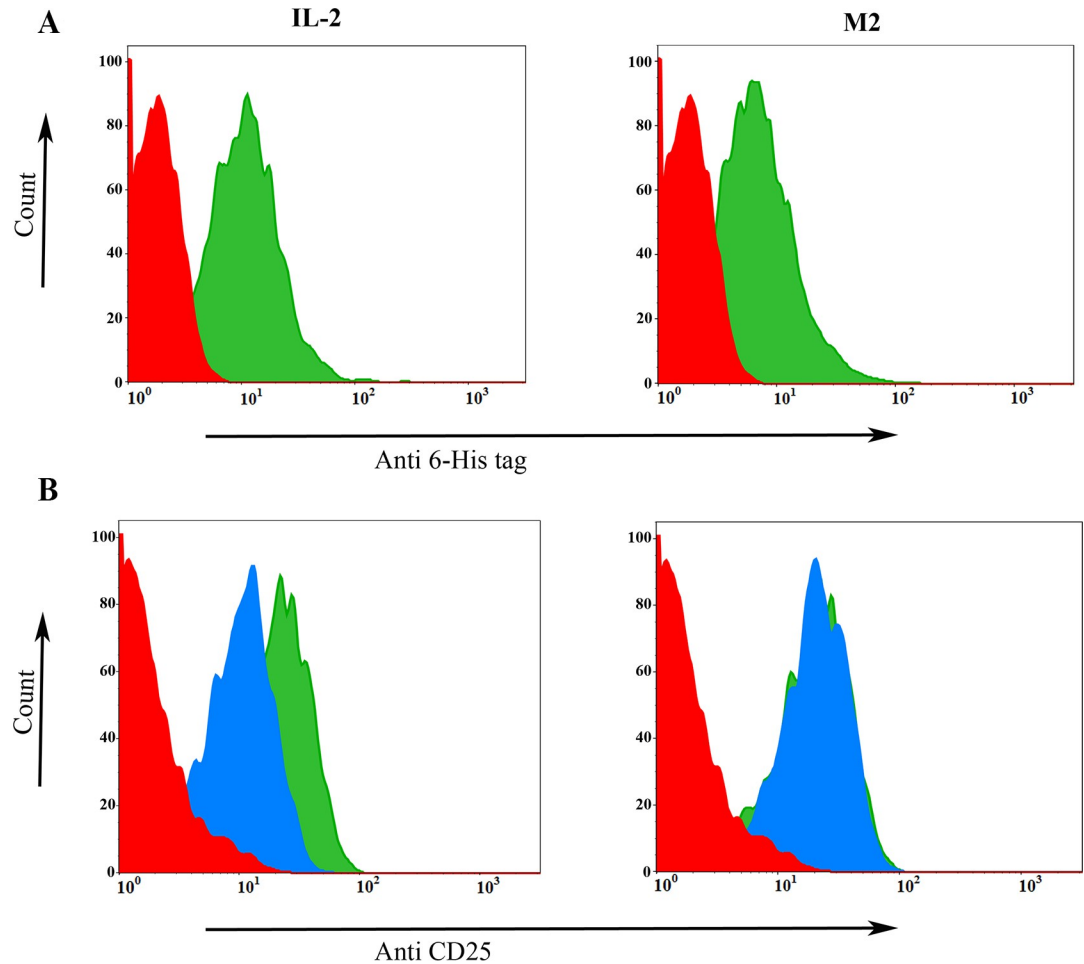


Fig 7. Flow cytometry analysis showing the binding ability of IL-2 mutein to the conA activated PBMC. A. Direct binding, red graph negative control, green graph wtIL-2 (left panel) and mutant IL-2 (right panel) bound to the cells and detected with rabbit anti-His-tag Ab and mouse anti-rabbit FITC-conjugated. B. Flow cytometry analysis showing the competitive assay. Negative control (red graph), cells labeled with anti-CD25 MAb-PE (green), and cells previously incubated with wtIL-2 (blue graph; left panel) or mutant IL-2 (blue graph; right panel) and then labeled with the anti-CD25 MAb-FITC.

<https://doi.org/10.1371/journal.pone.0264353.g007>

and broad application of IL-2 in the clinic [30]. It is therefore of considerable interest to find methods that improve IL-2 as an antitumor agent. Introducing targeted mutations to modifying IL-2 function is an interesting way through which the subsequent immune response can be controlled to favor suppressive or cytotoxic responses. Accordingly, mutations that decrease the affinity or interrupt CD25 binding are typically employed in order to preferentially stimulate cytotoxic CD8⁺ T and NK cells, while not affecting Tregs. Furthermore, the use of IL-2 muteins can disfavor contact with endothelial cells and significantly reduces the major side effect of HD-IL-2 immunotherapy, called vascular leak syndrome (VLS), which is caused by the direct binding of IL-2 to CD25⁺ pulmonary endothelial cells [31,32]. Pulmonary edema is caused by direct binding of IL-2 with the functional form of IL-2 receptors (IL-2R $\alpha\beta\gamma$ c) on lung endothelial cells and blocking the α -chain leads to dramatic reduction of the pulmonary toxicity induced by IL-2 [3].

It has already been reported that IL-2 interactions are mediated by two hydrophobic patches around F42, Y45, and L72 residues, located on A-B loop and helix B, and mutations in these residues result in loss of a large part of the Van der Waal interaction surface [34,35].

Heaton *et al.* have shown that secondary cytokine production, another cause of endothelial damage, is dramatically reduced by R38A and F42K muteins, which preferentially binds with an intermediate-affinity [33,34]. Such IL-2 variants provide an effective, yet less toxic means of cancer immunotherapy. This property is important because the high toxicity is the main drawback of IL-2 therapy. Another IL-2 mutein was generated by substitution of alanine at residues of R38, F42, Y45, and E62, resulting in decreased affinity for CD25 without affecting normal binding with IL-2R $\beta\gamma$ c [22]. The mutein inhibited the metastasis of the B16 melanoma variant MB16F0 and 3LL-D122 Lewis lung carcinoma in mice, while causing less toxic effects compared to wtIL-2 [3].

Following our *in-silico* simulations, two sets of triple mutations were assigned to wtIL-2 structure, both including F42A substitution located in the A-B loop. M1 also includes residues L72 and P65 that are parts of helix B. Mutations in F42A and P65A disturb the hydrophobic patch composed of aromatic rings shared by F42, P65, and Y45 residues (S5 Fig). Also, F42A and L72A substitutions eliminate the π -alkyl interactions with L42 and Y43 residues from IL-2R α (Fig 4D and 4E). Due to the loss of hydrophobic ridges around residues F42 and Y45, supported by the aromatic-aromatic interactions by P65 (Figs 1F and S5), the A-B loop cannot enter into the grooves between IL-2R α strands to stabilize the IL-2 and IL-2R α close to each other. Eventually, other interactions like Y45, T41, and D35 interactions that are located in more flexible regions of IL-2 (A-B loop and α) are lost as well.

Besides F42A substitution in M2 that avoids hydrophobic interactions establishment, the mutant includes K35A and E61A substitutions, located in α and B helices. Mutation in K35A disturbs hydrogen bond as well as salt bridge formation with residue E1 of IL-2R α and E61A substitution eliminates attractive charge interactions with K38. The obtained results show that K35A, F42A, and E61A further decrease the affinity for IL-2R α with a ΔG value of -40.3 kcal/mol in comparison to M1 and wtIL-2 with ΔG values of -55.2 and -67.8 kcal/mol, respectively. This energy difference in M1 and M2 can be attributed to the distribution of the mutations in the interacting regions. While mutations are assigned in the middle and top of the interacting region in M1, mutations in M2 are assigned throughout the region.

The performed *in vitro* experiments by flow cytometry indicated that the anti-CD25 mAb was able to bind to PBMC cells even after IL-2 mutant (M2) preincubation, therefore, the binding strength of the M2 to α -subunit is less than wtIL-2. Our results are in agreement with the previous investigation of the reduced capacity of the M2 compared to wtIL-2. Such mutations that severely reduce binding of α subunit, preferentially stimulate cytotoxic CD8⁺ T and NK cells while decrease interaction with Tregs and endothelial cells that resulted in low toxicity and are more effective in immunity than wtIL-2 [3,7,34,35].

5. Conclusions

Due to reduction in IL-2 binding to its receptor on high affinity cells, it was decided to reduce the affinity of IL-2 to its α -subunit by inserting mutations. A computational evaluation methodology was designed and employed with the aid of docking, molecular dynamic simulations and umbrella sampling technique to evaluate and identify mutations that would reduce the affinity of IL-2 to its natural subunit of IL-2R α . Accordingly, from the two triple mutants designed and studied, IL-2 mutant 2 (K35A, E61A, and F42A) showed noticeably a reduced affinity for IL-2R α . The computationally obtained results were further evaluated and confirmed with the aid of flow cytometry technique. Our experimental findings showed that the affinity of M2 has significantly reduced to high-affinity ConA activated PBMCs relative to wtIL-2. Therefore, further studies in this field should be continued. Also, the obtained results demonstrate that computer-aided design of single-site amino acid mutations is an applicable

strategy to modulate binding between two proteins with an already highly optimized interface and affinity in the nanomolar range.

Supporting information

S1 Fig. A diagram of the whole computational study procedure.

(TIF)

S2 Fig. Ramachandran plots of the final A. wtIL-2, B. Mutant 1, and C. Mutant 2, after 100 ns of MDs. Highly preferred, preferred and questionable observations are shown as green crosses, brown triangles, and red circles, respectively.

(TIF)

S3 Fig. The number of hydrogen bonds between wtIL-2 (green), M1 (blue) and M2 (magenta) with A. IL-2R β , B. IL-2R γ c, and C. IL-2R α .

(TIF)

S4 Fig. All umbrella sampling window simulations for, A. IL-2R α begins dissociation from wtIL-2 (green), B. IL-2R α begins dissociation from M1 (blue) and C. IL-2R α begins dissociation from M2 (magenta). D. The force on the spring over 500 ps of MDs for IL-2R α begins dissociation from wtIL-2 (green), M1 (blue) and M2 (magenta).

(TIF)

S5 Fig. The close view of the A-B loop and the grooves between IL-2R α strands, the hydrophobic ridges around residues F42, Y45, and L72 and their electrostatic interactions. The yellow spheres represent hydrophobic areas and the two end arrows represent electrostatic (like π - π , alkyl- π and π -cation) interactions.

(TIF)

S1 Table. The dissociation constants (Kd) and binding affinities (Δ G) of wt-IL-2 and the variants (after the point mutation assignment) for IL-2R α (calculated at 25°C).

(DOCX)

S2 Table. The percent of the residues in the favored, allowed and disallowed regions of the Ramachandran plots of the studied variants after 60 ns, 80 ns, and 100 ns of MDs.

(DOCX)

S3 Table. The dissociation constants (Kd) and binding affinities (Δ G) of the wt-IL2, M1 and M2 for IL-2R α , IL-2R β and IL-2R γ c (calculated at 25°C).

(DOCX)

Acknowledgments

The authors wish to express their deep gratitude to all who provided support during the course of this research.

Author Contributions

Conceptualization: Alireza Biglari, Mohammad Ali Shokrgozar, Sirous Zeinali, Yeganeh Talebkhan, Reza Ahangari Cohan.

Investigation: Arezoo Beig Parikhani, Rada Dehghan.

Methodology: Farhad Riazi Rad, Yeganeh Talebkhan.

Project administration: Kowsar Bagherzadeh.

Software: Arezoo Beig Parikhani, Kowsar Bagherzadeh.

Supervision: Sirous Zeinali, Soheila Ajdary, Mahdi Behdani.

Writing – original draft: Arezoo Beig Parikhani, Rada Dehghan.

Writing – review & editing: Kowsar Bagherzadeh, Yeganeh Talebkhan, Soheila Ajdary, Reza Ahangari Cohan, Mahdi Behdani.

References

1. Sun Z, Ren Z, Yang K, Liu Z, Cao S, Deng S, et al. A next-generation tumor-targeting IL-2 preferentially promotes tumor-infiltrating CD8⁺ T-cell response and effective tumor control. *Nat Commun.* 2019; 10: 1–12. <https://doi.org/10.1038/s41467-018-07882-8> PMID: 30602773
2. Liao W, Lin J-X, Leonard WJ. Interleukin-2 at the crossroads of effector responses, tolerance, and immunotherapy. *Immunity.* 2013; 38: 13–25. <https://doi.org/10.1016/j.immuni.2013.01.004> PMID: 23352221
3. Carmenate T, Pacios A, Enamorado M, Moreno E, Garcia-Martínez K, Fuente D, et al. Human IL-2 mutein with higher antitumor efficacy than wild type IL-2. *J Immunol.* 2013; 190: 6230–8. <https://doi.org/10.4049/jimmunol.1201895> PMID: 23677467
4. Stauber DJ, Debler EW, Horton PA, Smith KA, Wilson IA. Crystal structure of the IL-2 signaling complex: paradigm for a heterotrimeric cytokine receptor. *Proc Natl Acad Sci.* 2006; 103: 2788–93. <https://doi.org/10.1073/pnas.0511161103> PMID: 16477002
5. Rosenberg SA. IL-2: the first effective immunotherapy for human cancer. *Journal Immunol.* 2014; 192: 5451–8. <https://doi.org/10.4049/jimmunol.1490019> PMID: 24907378
6. Chelstrom LM, Finnegan D, Uckun FM. Treatment of BCL-1 Murine B-Cell Leukemia with Recombinant Cytokines: Comparative Analysis of the Anti-Leukemic Potential of Interleukin 1 Beta (IL-1 β), Interleukin 2 (IL-2), Interleukin-6 (IL-6), Tumor Necrosis Factor Alpha (TNF α), Granulocyte Colony Stimulating Factor (G-CSF), Granulocyte-Macrophage Colony Stimulating Factor (GM-CSF), and their Combination. *Leuk Lymphoma.* 1992; 7: 79–86. <https://doi.org/10.3109/10428199209053605> PMID: 1282065
7. Tang A, Harding F. The challenges and molecular approaches surrounding interleukin-2-based therapeutics in cancer. *Cytokine X.* 2019; 1: 100001.
8. Choudhry H, Helmi N, Abdulaal WH, Zeyadi M, Zamzami MA, Wu W, et al. Prospects of IL-2 in cancer immunotherapy. *Biomed Res Int.* 2018; 2018. <https://doi.org/10.1155/2018/9056173> PMID: 29854806
9. Ghasemi R, Lazear E, Wang X, Arefanian S, Zheleznyak A, Carreno BM, et al. Selective targeting of IL-2 to NKG2D bearing cells for improved immunotherapy. *Nat commun.* 2016; 7: 1–15. <https://doi.org/10.1038/ncomms12878> PMID: 27650575
10. Raggi G, Roldan N, Micallef V, Rapet A, De Maddalena L, Imler T, et al. Interleukin-2-induced vascular leak syndrome: clinically relevant in vitro recapitulation with a patient-derived lung-on-chip. *Eur Respir J.* 2020; 56: 4326.
11. Skrombolas D, Frelinger JG. Challenges and developing solutions for increasing the benefits of IL-2 treatment in tumor therapy. *Expert Rev Clin Immunol.* 2014; 10: 207–217. <https://doi.org/10.1586/1744666X.2014.875856> PMID: 24410537
12. Cesana GC, DeRaffele G, Cohen S, Moroziewicz D, Mitcham J, Stoutenburg J, et al. Characterization of CD4⁺ CD25⁺ regulatory T cells in patients treated with high-dose interleukin-2 for metastatic melanoma or renal cell carcinoma. *J Clin Oncol.* 2006; 24: 1169–1177. <https://doi.org/10.1200/JCO.2005.03.6830> PMID: 16505437
13. Farashi-Bonab S, Khansari N. Regulatory T cells in cancer patients and their roles in cancer development/progression. *MOJ Immunol.* 2014; 1: 00024.
14. Laskowski RA. PDBsum new things. *Nucleic Acids Res.* 2009; 37: D355–D359. <https://doi.org/10.1093/nar/gkn860> PMID: 18996896
15. Guex N, Peitsch MC. SWISS-MODEL and the Swiss-Pdb Viewer: an environment for comparative protein modeling. *Electrophoresis.* 1997; 18: 2714–2723. <https://doi.org/10.1002/elps.1150181505> PMID: 9504803
16. Kozakov D, Hall DR, Xia B, Porter KA, Padhorna D, Yueh C, et al. The ClusPro web server for protein–protein docking. *Nat Protoc.* 2017; 12: 255. <https://doi.org/10.1038/nprot.2016.169> PMID: 28079879

17. Pronk S, Páll S, Schulz R, Larsson P, Bjelkmar P, Apostolov R, et al. GROMACS 4.5: a high-throughput and highly parallel open source molecular simulation toolkit. *J Bioinform.* 2013; 29: 845–854. <https://doi.org/10.1093/bioinformatics/btt055> PMID: 23407358
18. Aliev AE, Kulke M, Khaneja HS, Chudasama V, Sheppard TD, Lanigan RM. Motional timescale predictions by molecular dynamics simulations: case study using proline and hydroxyproline sidechain dynamics. *Proteins.* 2014; 82: 195–215. <https://doi.org/10.1002/prot.24350> PMID: 23818175
19. Price DJ, Brooks CL III. A modified TIP3P water potential for simulation with Ewald summation. *J Chem Phys.* 2004; 121: 10096–10103. <https://doi.org/10.1063/1.1808117> PMID: 15549884
20. Kiwiel K, Murty K. Convergence of the steepest descent method for minimizing quasiconvex functions. *J Optim Theory Appl.* 1996; 89: 221–226.
21. Parrinello M, Rahman A. Polymorphic transitions in single crystals: A new molecular dynamics method. *J Appl Phys.* 1981; 52: 7182–7190.
22. York DM, Darden TA, Pedersen LG. The effect of long-range electrostatic interactions in simulations of macromolecular crystals: A comparison of the Ewald and truncated list methods. *J Chem Phys.* 1993; 99: 8345–8348.
23. Hess B, Bekker H, Berendsen HJ, Fraaije JG. LINCS: a linear constraint solver for molecular simulations. *J Comput Chem.* 1997; 18: 1463–1472.
24. Torrie GM, Valleau JP. Nonphysical sampling distributions in Monte Carlo free-energy estimation: Umbrella sampling. *Journal of Computational Physics.* 1977; 23:187–99.
25. Hub JS, De Groot BL, Van Der Spoel D. g_wham—A Free Weighted Histogram Analysis Implementation Including Robust Error and Autocorrelation Estimates. *J Comput Chem.* 2010; 6: 3713–3720.
26. Humphrey W, Dalke A, Schulten K. VMD: visual molecular dynamics. *J Mol Graph.* 1996; 14: 33–38. [https://doi.org/10.1016/0263-7855\(96\)00018-5](https://doi.org/10.1016/0263-7855(96)00018-5) PMID: 8744570
27. Makarewicz T, Kaźmierkiewicz R. Molecular dynamics simulation by GROMACS using GUI plugin for PyMOL. *J Chem Inf Model.* 2013; 53: 1229–34. <https://doi.org/10.1021/ci400071x> PMID: 23611462
28. Lovell SC, Davis IW, Arendall WB III, De Bakker PI, Word JM, Prisant MG, et al. Structure validation by C α geometry: ϕ , ψ and C β deviation. *Proteins.* 2003; 50: 437–450. <https://doi.org/10.1002/prot.10286> PMID: 12557186
29. Thornton AM, Shevach EM. CD4+ CD25+ immunoregulatory T cells suppress polyclonal T cell activation in vitro by inhibiting interleukin 2 production. *J Exp Med.* 1998; 188: 287–296. <https://doi.org/10.1084/jem.188.2.287> PMID: 9670041
30. Sim GC, Liu C, Wang E, Liu H, Creasy C, Dai Z, et al. IL2 variant circumvents ICOS+ regulatory T-cell expansion and promotes NK cell activation. *Cancer Immunol Res.* 2016; 4: 983–994. <https://doi.org/10.1158/2326-6066.CIR-15-0195> PMID: 27697858
31. Krieg C, Létourneau S, Pantaleo G, Boyman O. Improved IL-2 immunotherapy by selective stimulation of IL-2 receptors on lymphocytes and endothelial cells. *Proc Natl Acad Sci.* 2010; 107: 11906–11911. <https://doi.org/10.1073/pnas.1002569107> PMID: 20547866
32. Arenas-Ramirez N, Woytschak J, Boyman O. Interleukin-2: biology, design and application. *Trends Immunol.* 2015; 36: 763–777. <https://doi.org/10.1016/j.it.2015.10.003> PMID: 26572555
33. Heaton KM, Ju G, Grimm EA. Induction of lymphokine-activated killing with reduced secretion of interleukin-1 β , tumor necrosis factor- α , and interferon- γ by interleukin-2 analogs. *Ann Surg Oncol.* 1994; 1: 198–203. <https://doi.org/10.1007/BF02303524> PMID: 7842289
34. Heaton KM, Ju G, Grimm EA. Human interleukin 2 analogues that preferentially bind the intermediate-affinity interleukin 2 receptor lead to reduced secondary cytokine secretion: implications for the use of these interleukin 2 analogues in cancer immunotherapy. *Cancer Res.* 1993; 53: 2597–2602. PMID: 8495422
35. Vazquez-Lombardi R, Loetsch C, Zinkl D, Jackson J, Schofield P, Deenick EK, et al. Potent antitumour activity of interleukin-2-Fc fusion proteins requires Fc-mediated depletion of regulatory T-cells. *Nat Commun.* 2017; 8: 1–12. <https://doi.org/10.1038/s41467-016-0009-6> PMID: 28232747